JCI insight

RESEARCH ARTICLE

Nrf2 activation protects against lithium-induced nephrogenic diabetes insipidus

Soma Jobbagy,[1] Dario A. Vitturi,[1,2] Sonia R. Salvatore,[1] Maria F. Pires,[1] Pascal Rowart,[1] David R. Emlet,[3] Mark Ross,[4] Scott Hahn,[2] Claudette St. Croix,[4] Stacy G. Wendell,[1,5] Arohan R. Subramanya,[6] Adam C. Straub,[1,2] Roderick J. Tan,[6] and Francisco J. Schopfer[1]

[1]Department of Pharmacology and Chemical Biology, [2]Pittsburgh Heart, Lung and Blood Vascular Medicine Institute, [3]Center for Critical Care Nephrology, Department of Critical Care Medicine, [4]Center for Biologic Imaging, [5]Health Sciences Metabolomics and Lipidomics Core, and [6]Department of Medicine, Renal-Electrolyte Division, University of Pittsburgh, Pittsburgh, Pennsylvania, USA.

Lithium (Li) is the mainstay pharmacotherapeutic mood stabilizer in bipolar disorder. Its efficacious use is complicated by acute and chronic renal side effects, including nephrogenic diabetes insipidus (NDI) and progression to chronic kidney disease (CKD). The nuclear factor erythroid-derived 2–related factor 2 (Nrf2) pathway senses and coordinates cellular responses to oxidative and electrophilic stress. Here, we identify that graded genetic activation of Nrf2 protects against Li-induced NDI (Li-NDI) and volume wasting via an aquaporin 2–independent mechanism. Renal Nrf2 activity is differentially expressed on functional segments of the nephron, and its activation along the distal tubule and collecting duct directly modulates ion transporter expression, mimicking paradoxical effects of diuretics in mitigating Li-NDI. In addition, Nrf2 reduces cyclooxygenase expression and vasoactive prostaglandin biosynthesis. Pharmacologic activation of Nrf2 confers protective effects, confirming this pathway as a potentially novel druggable target for the prevention of acute and chronic renal sequelae of Li therapy.

Introduction

For over 60 years, lithium (Li) has been the gold-standard agent for prophylaxis and treatment of bipolar disorder. Its efficacy in acute treatment and chronic prevention of both manic and depressive episodes make it the first-line drug administered for long-term mood stabilization, and it remains the only therapeutic that is documented to reduce the incidence of suicide-related events (1). Complicating its psychopharmacologic benefits, Li exhibits a narrow therapeutic index and may cause cardiovascular, neurological, and renal sequelae (2). Development of nephrogenic diabetes insipidus (NDI) is the most prevalent renal side effect of chronic Li administration, with over 50% of patients developing hyposthenuria and 20%–40% of patients developing frank NDI with overt polyuria (3, 4). In addition to reducing quality of life, Li-induced NDI (Li-NDI) in the long term poses a more severe iatrogenic risk, as it correlates with increased progression to chronic kidney disease (CKD) and, ultimately, renal failure (5–11).

In murine models, Li has been demonstrated to target the epithelium lining the distal tubule (DT) and collecting duct (CD) of the nephron, where its uptake is mediated by the epithelial sodium channel (ENaC) (12–14) and where it induces loss of function through uncoupling the effects of arginine vasopressin and downregulating aquaporin 2 (AQP2) to yield pronounced polyuria with compensatory polydipsia (15–17).

Several recent publications have implicated renal hyperactivation of nuclear factor erythroid-derived 2–related factor 2–dependent (Nrf2-dependent) signaling in the development of NDI (18, 19). Nrf2 is a basic leucine zipper transcription factor that controls transcriptional responses to oxidative and electrophilic insults through upregulation of cytoprotective gene expression (20–23). Under non-stressed conditions, Nrf2 is retained in the cytosol and is rapidly targeted for proteasomal degradation by the Kelch like-ECH–associated protein 1 (Keap1)/Cullin3 (Cul3) complex. Redox-sensitive cysteine thiols in Keap1 sense cellular exposure to oxidative or electrophilic stress. Oxidation or alkylation of these residues derepress Nrf2 transcriptional activity (23–25). Specifically, both a nonlethal model of a global genetic Nrf2 suppressor Keap1-KO and kidney epithelium Keap1–deficient mice result in severe NDI with strong downregulation of AQP2 (18, 19). Inducible renal tubular deletion of the E3 ubiquitin

Conflict of interest: DAV, SGW, and FJS have financial interest in Complexa Inc.

Submitted: March 8, 2019
Accepted: November 20, 2019
Published: January 16, 2020.

Reference information: *JCI Insight*. 2020;5(1):e128578. https://doi.org/10.1172/jci.insight.128578.

ligase Cul3 — which is responsible for regulating both NaCl reabsorption via WNK/SPAK signaling and promoting Keap1-assisted Nrf2 ubiquitination and degradation — not only activates WNK signaling, but also causes NDI with loss of AQP2 (26). Similarly, genetic ablation or pharmacologic inhibition of the accessory Nrf2 repressor glycogen synthase kinase 3 β (GSK3β) downregulates AQP2 (27), while in vitro observations support that Li can inhibit GSK3β and consequently activate Nrf2 (28–30).

In contrast to the above results that suggest a correlation between Nrf2 hyperactivation and NDI development, partial genetic and small-molecule pharmacologic activation of Nrf2 have been found to protect against renal injury in diverse models of acute kidney injury (AKI) and CKD (31–36). Moreover, promising Phase II/III clinical trials are underway, targeting Nrf2 to protect the kidney against CKD (37–40). Current treatments of Li-NDI include sodium chloride cotransporter–blocking (NCC-blocking) agents (e.g., thiazides) (41–45), ENaC inhibitors (e.g., amiloride) (12–14, 46–49), carbonic anhydrase inhibitors (e.g., acetazolamide) (50–52), and nonsteroidal antiinflammatory drugs (NSAIDs; e.g., indomethacin) (53–56). The use of each of these agents to improve Li-NDI is paradoxical, as these compounds are used in other contexts to induce diuresis (thiazides, ENaC inhibitors, CA inhibitors) or are contraindicated in patients with renal disease (NSAIDs). Furthermore, the mechanisms of action of these drugs are incompletely understood, as a reduction in polyuria/polydipsia is not consistently attributable to improvement of urine osmolality and AQP2 expression.

In this context, we evaluated whether direct activation of Nrf2 signaling is operative in a murine model of Li-NDI. We found that Nrf2 signaling was neither induced by Li nor necessary for the development of NDI. Instead, graded genetic activation of Nrf2 in the Keap1 hypomorphic ($Keap1^{hm}$) mouse model (57) completely protected against development of Li-NDI and its characteristic polydipsia and polyuria. The mechanism includes modulation of ion channel expression and cyclooxygenase (COX) expression and activity. Significantly, the protection occurred independently of AQP2 and without altering plasma Li concentration. Pharmacologic activation of Nrf2 with the electrophile bardoxolone methyl (CDDO-Me) likewise showed protection in this model of Li-NDI, providing proof of concept for a potentially novel druggable pathway for NDI prophylaxis in the setting of Li use.

Results

Dietary administration of Li leads to rapid development of NDI without inducing renal Nrf2 targets. To establish a murine model of NDI, mice were administered control chow diet or 0.17% LiCl diet for 0–7 days (Figure 1A), during which body weight, food intake (Supplemental Figure 1, A and B; supplemental material available online with this article; https://doi.org/10.1172/jci.insight.128578DS1), and water intake (Figure 1B) were monitored. Water intake, used as a surrogate measurement for micturition to avoid the impact of the stress associated with metabolic cages (58), was significantly increased in mice receiving LiCl after 4 days. By 7 days, LiCl treatment significantly downregulated renal expression of AQP2 that corresponded with a significant hyposthenuria (Figure 1, C and D, and Supplemental Figure 1C), without impacting transcript levels of the Nrf2 gene targets NADPH quinone oxidoreductase 1 (NQO1), heme oxygenase 1 (HO-1), or γ-glutamyl cysteinyl ligase modulatory subunit (GCLM) (Supplemental Figure 1D). NQO1 protein abundance was likewise unchanged (Figure 1E). Mice developed significant hypernatremia and polycythemia when water intake was clamped to match baseline intake during LiCl treatment (Supplemental Figure 2), indicating that the model recapitulated NDI and not Li-induced primary polydipsia. While Li did not modify Nrf2 signaling activity, a large dynamic range of NQO1 expression was observed between $Keap1^{hm}$ and Nrf2–KO ($Nrf2^{-/-}$) mice (Figure 1E). To test whether Li exerted a cell-specific effect on Nrf2 activity, which could have been masked in whole-tissue analysis, NQO1 expression was evaluated by immunofluorescence microscopy. These studies likewise revealed no modulation of Nrf2 activity by Li (Figure 1F and Supplemental Figure 3). To further confirm the absence of Li-induced Nrf2 modulation, NQO1 expression was determined in immunoaffinity isolated primary human renal cortical cells representing proximal tubule (PT; $CD13^+$) and DT ($Muc1^+$) cell populations (59). Incubation of PT and DT cells from 3 distinct human donors incubated with Li (10 and 50 mM) did not modulate NQO1 expression in either cell type (Figure 1G).

Nrf2 is not necessary for development of Li-NDI in mice. To additionally test if Nrf2 activation is required for Li-NDI development, Li administration was repeated in mice with a global KO of Nrf2. $Nrf2^{-/-}$ mice displayed a 90% reduction in renal NQO1 and were slightly oliguric at baseline (Supplemental Figure 4, A and B). $Nrf2^{-/-}$ mice were maintained on control diet for 5 days, followed by Li diet for 6 days (Figure 2A). As in WT, Li modestly reduced body weight (Figure 2B). Food intake was transiently suppressed in the first 3 days of LiCl diet administration but rebounded to baseline by 4 days (Figure 2C). Despite Nrf2

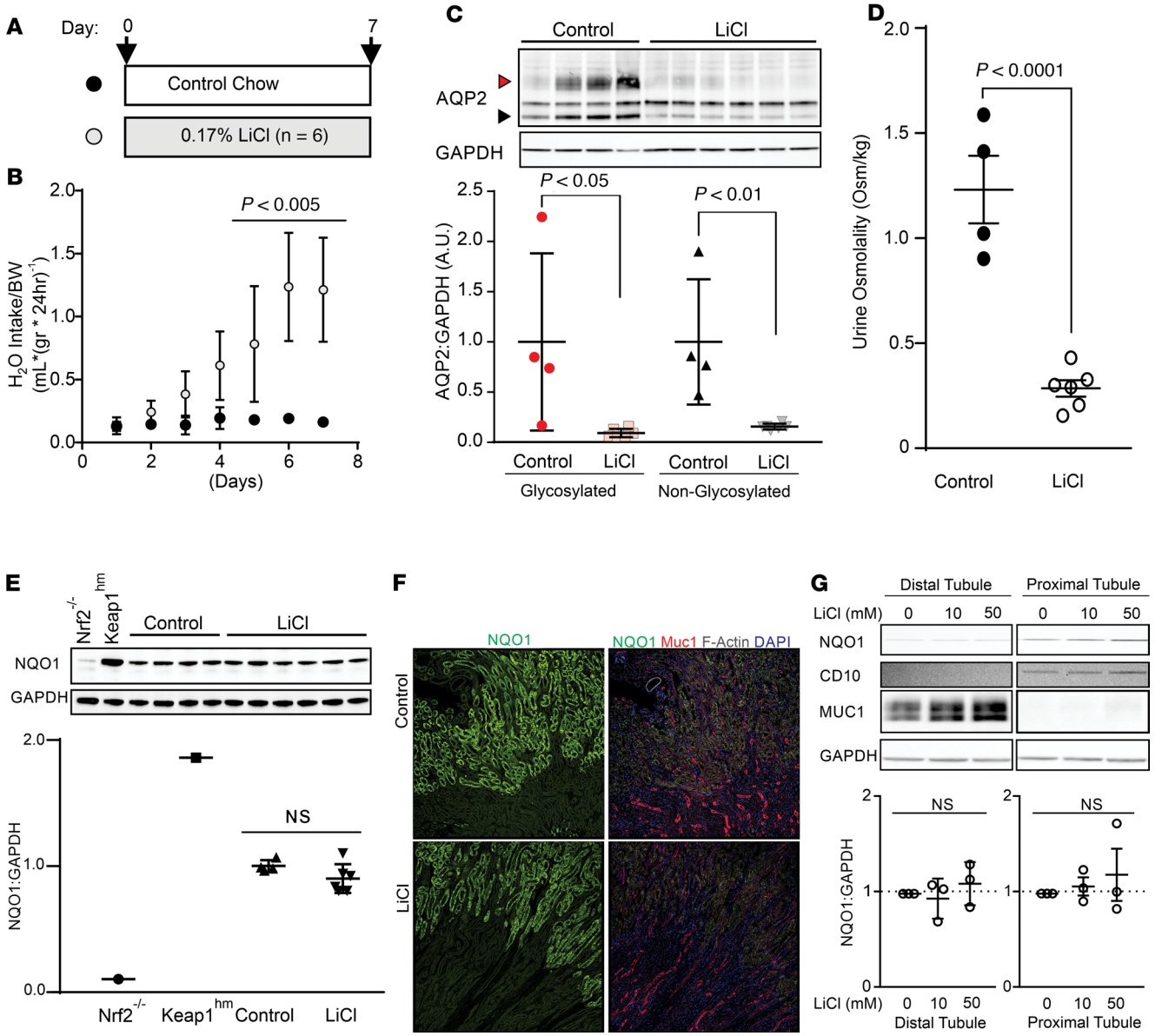

Figure 1. Lithium administration rapidly induces NDI but does not activate renal Nrf2 signaling. (**A**) Schematic of experimental Li-NDI model. Mice received normal chow (control) or 0.17% dietary LiCl (LiCl) for 0–7 days. (**B**) Water intake was significantly increased after Li administration. Results plotted as mean ± SD of 4 (control) or 6 (LiCl) animals per group and statistical significance assessed by 2-way ANOVA with Dunnett correction for multiple comparisons. (**C**) Immunoblotting and densitometry for glycosylated (red arrowhead, 30–42 kDa) and nonglycosylated (black arrowhead, 24 kDa) AQP2 expression in kidney homogenates. Full blot is shown in Supplemental Figure 1C. (**D**) Spot urine osmolality from day 7. (**E**) Immunoblotting and densitometry for NQO1 protein expression in kidneys from Nrf2$^{-/-}$, Keap1^{hm}, control, and LiCl-fed mice. (**F**) Immunofluorescence microscopy evaluating NQO1 (green) and Muc1 (red) protein abundance, with F-actin (phalloidin, white) and DAPI (blue) costains in WT mouse kidney. Expanded images shown in Supplemental Figure 3. Images captured as 3 × 3 image stitch; original magnification, 20×. (**G**) Representative immunoblotting for NQO1 in primary human renal cortical cells immunoaffinity enriched for Muc1 or CD13 and cultured in presence of 10 or 50 mM LiCl for 6 hours. Densitometry shows average results of 3 experiments on primary human renal cortical cell lines from 3 independent donors and normalized to internal vehicle control; NS, not statistically significant by 1-way ANOVA with Tukey correction for multiple comparisons comparing to vehicle control.

ablation, dietary Li induced NDI with temporally similar onset of polydipsia (Figure 2D) as in WT mice (Figure 1B). Urine osmolality was also significantly reduced (7-fold) compared with WT control (Figure 2E), indicating that Nrf2 signaling is not required for development of NDI.

Keap1 hypomorphism induces a distinct phenotype from complete global or kidney-specific KO. Hyperactivation of Nrf2 through genetic ablation of the E3 ubiquitin ligase complex proteins Keap1 or Cul3 has been shown to induce NDI in mice (18, 19, 26). By contrast, Keap1^{hm} mice had an increase in

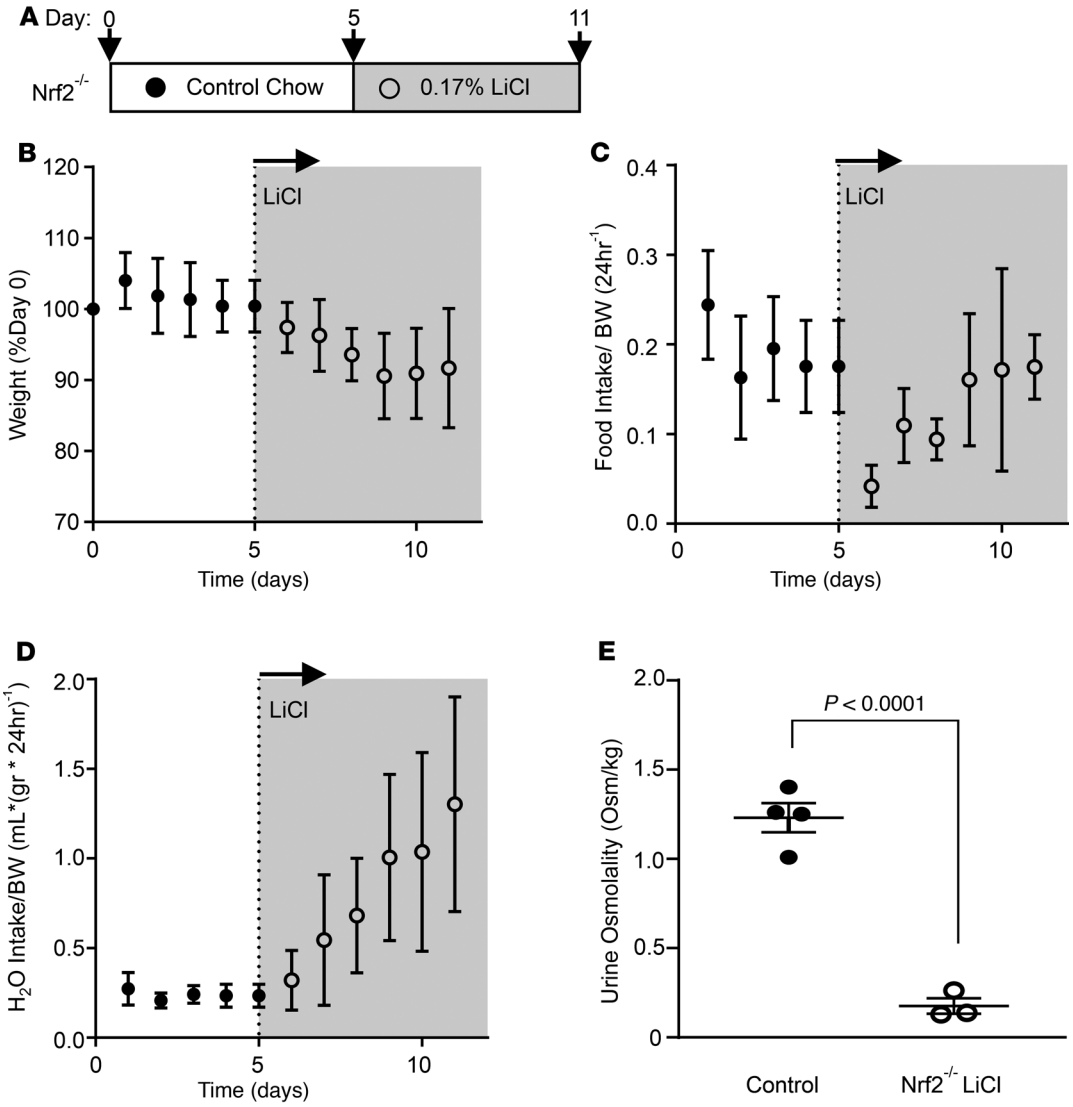

Figure 2. Nrf2 is not required for development of Li-NDI. (**A**) Schematic of experiment. (**B–D**) Animal weight (**B**), 24-hour body weight-normalized food intake (**C**), and water intake (**D**) of Nrf2$^{-/-}$ mice on control diet (0–5 days) followed by LiCl diet (6–11 days). (**E**) spot-urine osmolality of LiCl-treated Nrf2$^{-/-}$ or WT control mice at day 11. Statistical analysis by *t* test, $P < 0.05$ considered significant.

kidney mass (Supplemental Figure 5A) but no hydronephrosis. Under basal conditions, Keap1^{hm} mice were found to be mildly hyposthenuric (Supplemental Figure 5B). However, upregulation of plasma renin was normal, and urine concentration in response to 12-hour water deprivation was no different from WT (Supplemental Figure 5, C and D). This indicates that, while kidney function is markedly impaired by complete ablation of Nrf2 repressors (18, 19, 26), graded Nrf2 activation in the Keap1^{hm} is not pathogenic.

Graded activation of Nrf2 rescues Li-NDI in mice. Next, Li was administered to WT and Keap1^{hm} mice to test whether Nrf2 and Li induced NDI via synergistic mechanisms (Figure 3A). To our surprise, instead of exacerbating the renal toxicity of Li, activation of Nrf2 signaling conferred significant protective effects.

After 3 days, WT-Li mice exhibited a modest (~5%) reduction in body weight, while Keap1^{hm} mice receiving Li were protected and demonstrated no change when compared with control diet (Figure 3B), despite identical food intake throughout the observation period (Figure 3C). As in our validation studies, Li intake in the WT cohort recapitulated the polydipsia of NDI (Figure 1B and Figure 3D) and correlated with polyuria. Strikingly, Keap1^{hm} mice receiving Li failed to develop polyuria, and blood chemistry revealed no differences in plasma Na^+, K^+, or Cl^- between groups, suggesting that thirst mechanisms were sufficiently present in each of the experimental groups (Figure 3, E–G). Plasma Li^+

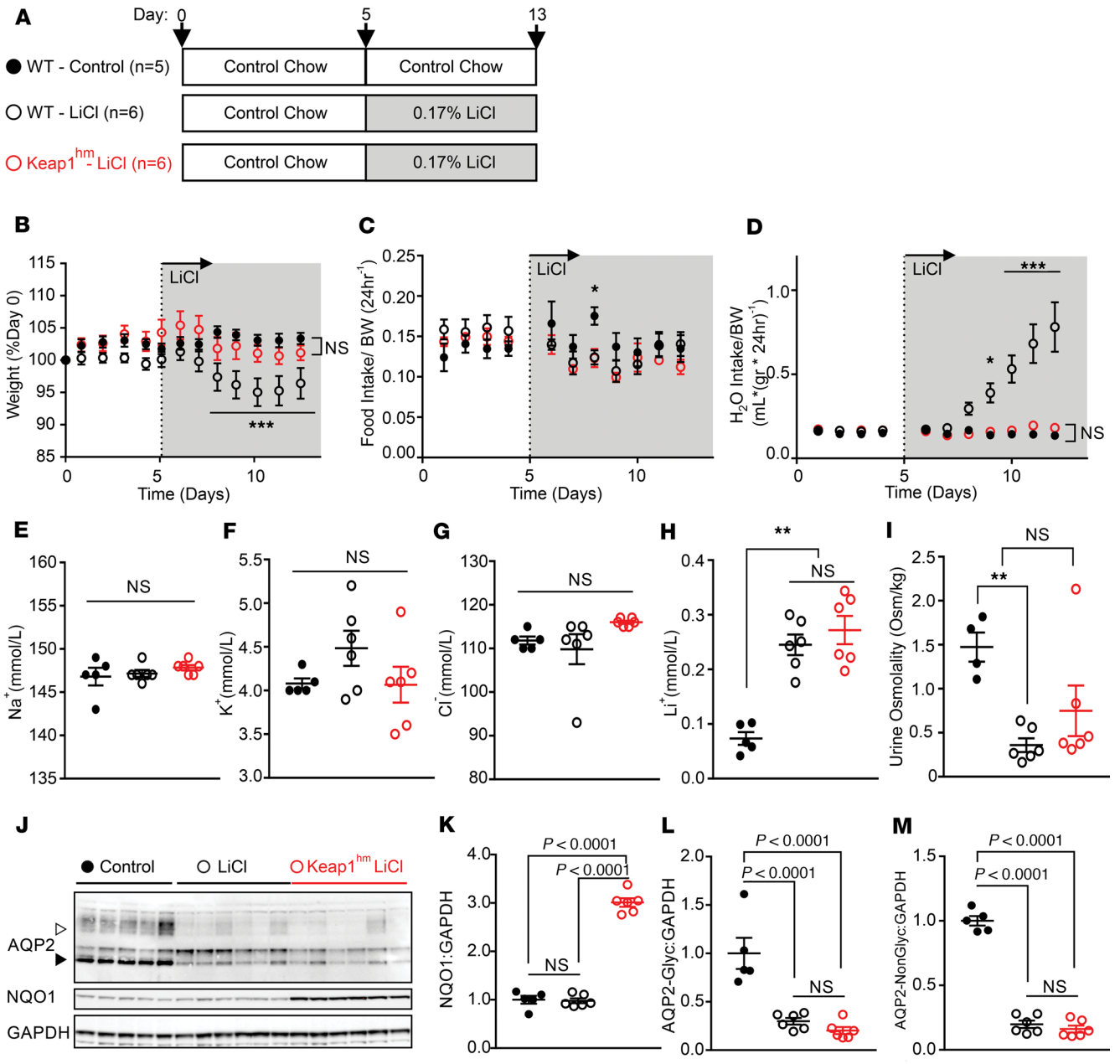

Figure 3. Nrf2 hyperactivation protects against development of Li-NDI. (**A**) Schematic of the animal model of Li-NDI showing groups and *n* per group. (**B**) Animal weight changes as a function of time, normalized to starting weight. (**C** and **D**) Twenty-four–hour body weight–normalized food intake (**C**) and water intake (**D**). Results plotted as mean ± SEM, $^{*}P < 0.05$ and $^{***}P < 0.001$ denote statistical significance by 2-way ANOVA with Dunnett correction for multiple comparisons; means of each time point compared with control. (**E**–**H**) Plasma sodium (**E**), potassium (**F**), chloride (**G**), and Li^{+} (**H**). (**I**) Urine osmolality from day 12. (**J**) Immunoblotting for glycosylated (white arrowhead, 30–42 kDa) and nonglycosylated (black arrowhead, 24 kDa) AQP2 and NQO1 expression in kidney homogenates. Full blot shown in Supplemental Figure 4, C and D. (**K**–**M**) Densitometry showing individual values; *n* = 5–6, mean ± SEM with statistical analysis by 1-way ANOVA with Tukey correction for multiple comparisons.

was equally elevated in both WT and Keap1^{hm} groups (Figure 3H), consistent with equivalent absorption, exposure, and clearance of Li.

The WT-Li cohort had significantly lower spot urine osmolality than the control diet cohort (Figure 3I), indicating that polyuria was accompanied by hyposthenuria, consistent with NDI. Urine osmolality was likewise reduced in the Keap1^{hm}-Li cohort compared with control and was not significantly different from WT-Li (Figure 3I). Plasma renin activity, as a readout for physiological response to plasma volume, was identical across experimental groups, suggesting that all mice were euvolemic and drinking to satiety (Supplemental Figure 6A). Importantly, plasma blood urea nitrogen (BUN) was unaffected by genotype

or Li exposure, indicating that any changes caused by the Keap1^{hm} genotype did not have a deleterious effect on renal function (Supplemental Figure 6B).

Expression of NQO1 was not affected by Li treatment but was significantly increased in Keap1^{hm} animals, confirming constitutive activation of Nrf2 (Figure 3, J and K, and Supplemental Figure 7A). Glycosylated ~30–42 kDa (Figure 3, J and L, white arrowhead; and Supplemental Figure 7B) and nonglycosylated 24 kDa (Figure 3, J and M, black arrowhead; and Supplemental Figure 7B) isoforms of AQP2 were significantly reduced by Li exposure in both groups, consistent with NDI. Surprisingly, AQP2 expression did not correlate with volume intake in Keap1^{hm} mice.

AQP1 is a critical water-permeable channel expressed along both apical and basolateral membranes of multiple nephron segments, including the PT, descending loop of Henle, and epithelium of the vasa recta (60). To determine if increased non-AQP2 passive water transporter abundance was responsible for reduction in polydipsia/polyuria in Keap1^{hm} mice, expression of AQP1 was evaluated. AQP1 expression was significantly decreased by Li treatment, a response not further modified by Nrf2 activation (Supplemental Figure 7C)

Nrf2 modulates renal ion channel and transporter expression. Clinically, established Li-NDI is treated with inhibitors of the NCC, ENaC, CA, or with NSAIDs, which inhibit prostaglandin biosynthesis.

Thiazide diuretics exhibit a paradoxical antidiuretic effect when administered to experimental animals or patients with NDI (41–45). Similar to our observations in Li-treated Keap1^{hm} (Figure 3), thiazide-induced reduction in polyuria occurs without proportionate rescue of urine osmolality (43–45). Thus, we hypothesized that hyperactivation of Nrf2 might downregulate the abundance and/or activity of the thiazide-sensitive sodium transporter NCC. Total protein expression of NCC (tNCC) was reduced in the Keap1^{hm}-Li cohort, while activation of NCC through phosphorylation at threonine 53 (pNCC [T53]:tNCC ratio) was significantly reduced by Li but not affected by Keap1 hypomorphism (Figure 4, A–D, and Supplemental Figure 8, A and B). NCC abundance was likewise reduced in Li-naive Keap1^{hm} animals (Supplemental Figure 9A). To evaluate phosphorylation, mice were subjected to sodium deprivation, which appropriately increased pNCC in both genotypes (Supplemental Figure 9B). This suggests that hyperactivation of Nrf2 reduces NCC protein levels but not its activation. The loop diuretic furosemide, which targets the sodium-potassium cotransporter NKCC2, has also been found to exert paradoxical antidiuretic effects in Li-NDI (61), although this discovery has not translated to widespread clinical use. Akin to effects on NCC, NKCC2 expression was downregulated by Li and further reduced in the Keap1^{hm}-Li cohort (Figure 4, A and E, and Supplemental Figure 8C).

Amiloride reduces polyuria in murine models of Li-NDI, as well as in human patients, through reduction of ENaC-mediated uptake of Li (12–14, 46–49). No differences were observed between expression of ENaC subunits α, β, or γ in Li-treated WT and Keap1^{hm} animals, suggesting that regulation of this transporter was not involved in Nrf2-mediated resistance to NDI (Figure 4, A and F–H, and Supplemental Figure 8, D–F). Likewise, Li reduced expression of another therapeutic target, CA-II (50–52), in WT animals, with an additional reduction in Keap1^{hm}-Li mice (Figure 4I and Supplemental Figure 8G). Reduction in NKCC2 or CA-II abundance was not observed in Li-naive Keap1^{hm} mice (Supplemental Figure 9A)

It has been suggested that chronic Li exposure may induce transdifferentiation of CD principal cells to intercalated cells (62, 63). After 1 week of Li, abundance of the H^+-ATPase B1 subunit ATP6V1B1 remained unchanged but was significantly reduced by Keap1 hypomorphism (Supplemental Figure 8H). Collectively, these data suggest that protection from Li-NDI in Keap1^{hm} mice is at least partially due to reduced NCC, with additional contribution from Li-dependent changes in NKCC2 and CA-II abundance.

Renal effects of graded genetic and pharmacologic activation of Nrf2 are localized to the DT. Despite extensive research evaluating Nrf2 as a pharmacologic target for renal diseases, the distribution and sensitivity of Nrf2 signaling activity in the kidney have not been well characterized. Immunofluorescence microscopy was performed on kidney sections from WT mice probing for the Nrf2 target NQO1 and the marker Mucin 1 (MUC1), which is expressed in the distal convoluted tubule, connecting tubule, and collecting system (64–66). NQO1 was found to be highly expressed in the renal cortex, with localization to the PTs that stained negative for MUC1. By contrast, glomeruli, vessels, MUC1$^+$ distal/connecting tubules, and the renal medulla displayed low expression of NQO1 (Figure 5, A and B).

NQO1 staining of kidneys from Keap1^{hm} mice showed upregulation of NQO1 in tubule segments with low Nrf2 activity in WT counterparts, but this was not shown in glomeruli or vessels.

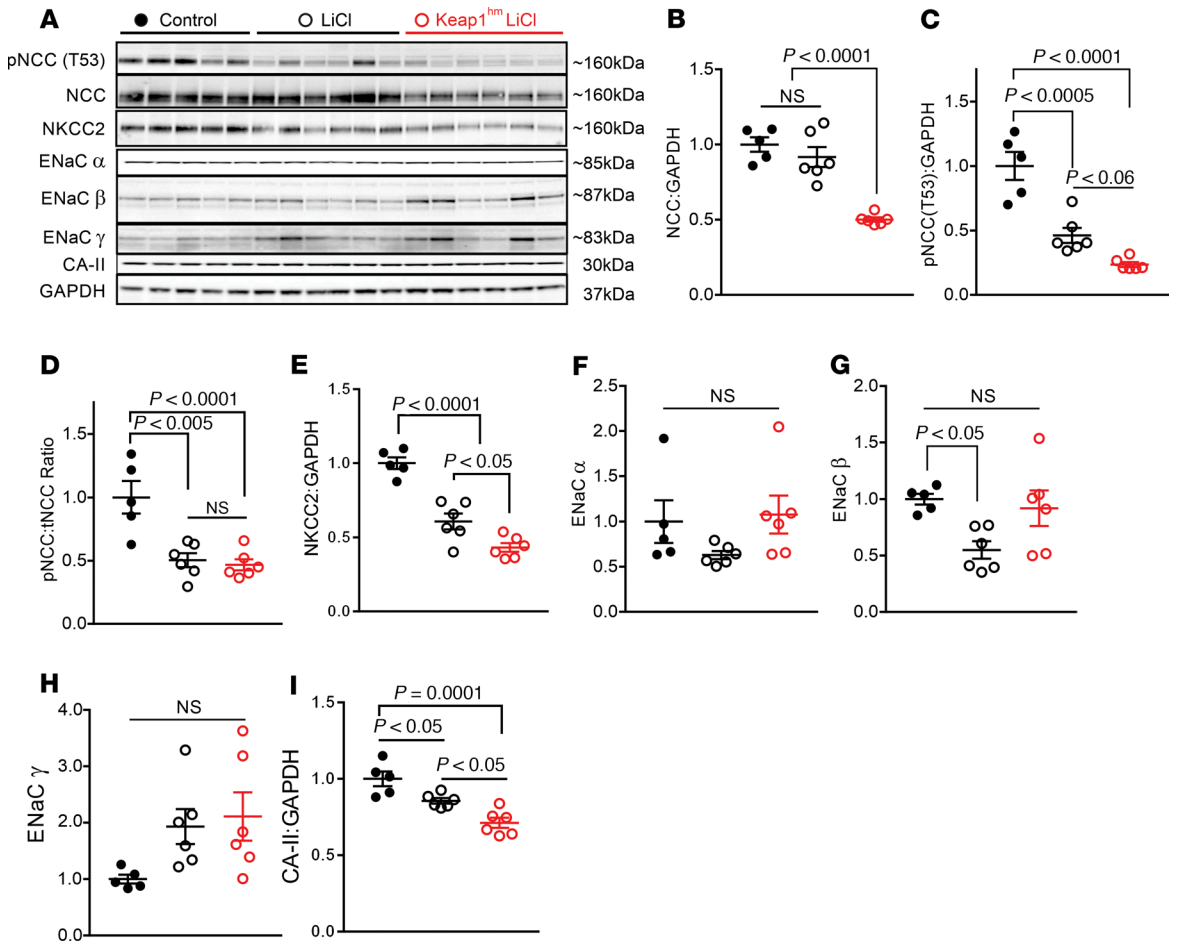

Figure 4. Nrf2 hyperactivation downregulates NCC and CA-II, but not ENaC, expression. (**A**) Immunoblotting of kidney lysates; each lane represents 1 animal from the study. (**B–I**) Densitometric analysis of immunoblots normalized to GAPDH showing individual values; mean ± SEM. Statistical analysis by 1-way ANOVA with Tukey correction for multiple comparisons. Full blots shown in Supplemental Figure 5.

Significantly, coexpression of MUC1 and NQO1 was observed in the cortex, suggesting an increase of Nrf2 activity in the distal/connecting tubules. NQO1 abundance was found to be increased in both the outer and inner renal medulla of Keap1^{hm} animals (Figure 5C). To further test the distribution of Nrf2 and sensitivity to activation in a translational model, NQO1 expression was determined in primary human renal cortical cells representing PT and DT cell populations (59) in the presence or absence of the Nrf2 activator CDDO-Imidazolide (CDDO-Im) (Figure 5, D–G). Supporting the observations made in mice, NQO1 expression was significantly higher in PT than in DT. Recapitulating the effects of genetic activation of Nrf2 in Keap1^{hm} mice, NQO1 expression did not further increase upon exposure to CDDO-Im in CD10$^+$/CD13$^+$ HAK cells, whereas the MUC1$^+$ cells responded robustly with 3-fold elevation in NQO1. Taken together, these observations support a model of high basal Nrf2 activity in the PT and sensitivity to genetic or pharmacologic induction in the distal convoluted tubule and collecting system (Figure 5H).

Nrf2 inhibits vasoactive prostaglandin synthesis via attenuation of COX expression. While the exact mechanism remains unclear, the paradoxical protection afforded by diuretics in Li-NDI is thought to involve tubuloglomerular feedback (TGF), leading to a reduction of glomerular filtration rate (GFR) and increased proximal tubular solute reabsorption. Thiazides and acetazolamide dramatically diminish polyuria induced by Li but have only marginal effects on AQP2 abundance and urine osmolality (44, 45, 50, 51).

TGF is a direct result of paracrine and endocrine signaling from the macula densa at the apex of the ascending limb of the loop of Henle to induce vasoconstriction of afferent arterioles to fine-tune glomerular filtration. Both the renin-angiotensin-aldosterone signaling (RAAS) and prostaglandin signaling has been implicated in this process (55, 56). We previously showed that RAAS was unaffected by

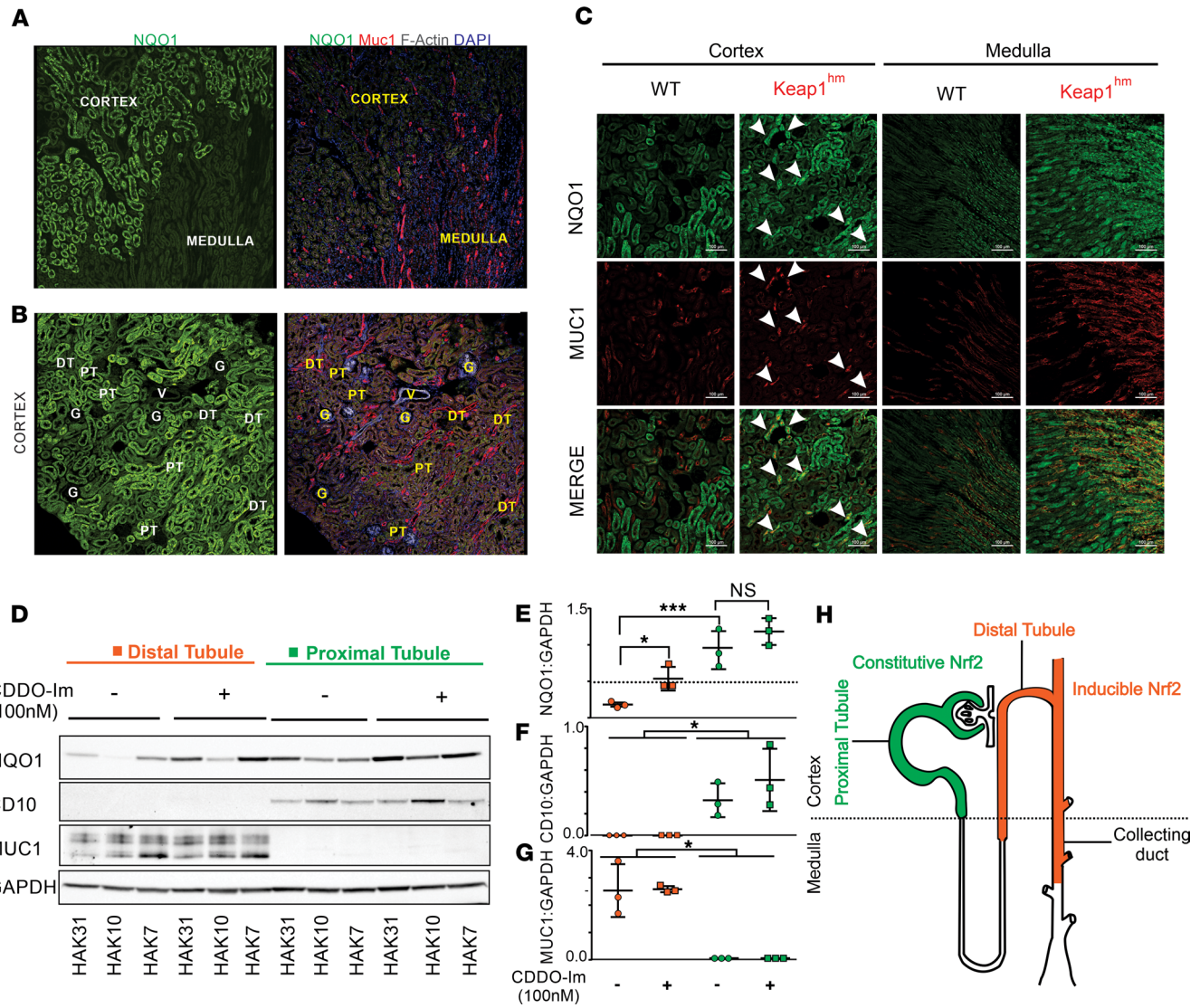

Figure 5. Distribution of Nrf2 activity marker NQO1 and inducibility in murine kidney and cultured primary human kidney epithelial cells. (**A** and **B**) Immunofluorescence staining in WT mouse kidney for NQO1 (green), Muc1 (red), F-actin (white), and DAPI (blue) showing cortical predominance and proximal tubular enrichment of Nrf2 activity. DT, distal tubule; PT, proximal tubule; G, glomerulus; V, vessel. Images captured as 3 × 3 image stitch, original magnification, 20×. (**C**) Immunofluorescence staining for NQO1 (green) and Muc1 (red) in renal cortex and medulla reveals increased cortical colocalization and increased medullary expression in Keap1^{hm} mice. Original magnification, 20×. Scale bar: 100 μm. (**D**) Expression of NQO1 in immunoaffinity isolated primary human distal and proximal tubule epithelial cells from renal cortex of 3 independent donors (HAK31, HAK10, and HAK7) after CDDO-Im treatment. (**E**–**G**) Densitometry for NQO1 (**E**), CD10 (**F**), and MUC1 (**G**) normalized to GAPDH expression. Results are mean ± SEM of 3 replicates, each representing a unique human sample. Statistical testing by 1-way ANOVA; significance denotes *$P < 0.05$; ***$P < 0.0005$. (**H**) Schematic showing distribution of constitutive and inducible Nrf2 activity in kidney.

Nrf2 hyperactivation (Supplemental Figure 5D). To test the role of prostaglandins in this pathway, renal COX expression and prostaglandin biosynthesis were evaluated.

COX-1 (Figure 6, A and B) and COX-2 (Figure 6, A and C) expression were found to be reduced in Keap1^{hm}-Li mice, suggesting that Nrf2 activation has direct effects on renal expression of these proteins. Because Li was additionally found to downregulate COX-1 and COX-2 in WT mice, the experiment was repeated, comparing tissues from WT and Keap1^{hm} mice on control diet, which confirmed a significant reduction in renal COX-1 and COX-2 mRNA and protein levels by Nrf2 activation (Supplemental Figure 10, A–C). Downregulation of COX-2 in Keap1^{hm} mice was further evaluated by immunohistochemical staining of kidney sections (Supplemental Figure 10D). Kidneys from Nrf2$^{-/-}$ animals showed marginally increased COX-1 and COX-2 expression compared with control (Supplemental Figure 10, E and F), showing additional indirect regulation of COX-1 and COX-2 by Nrf2 signaling. The downregulation of COX

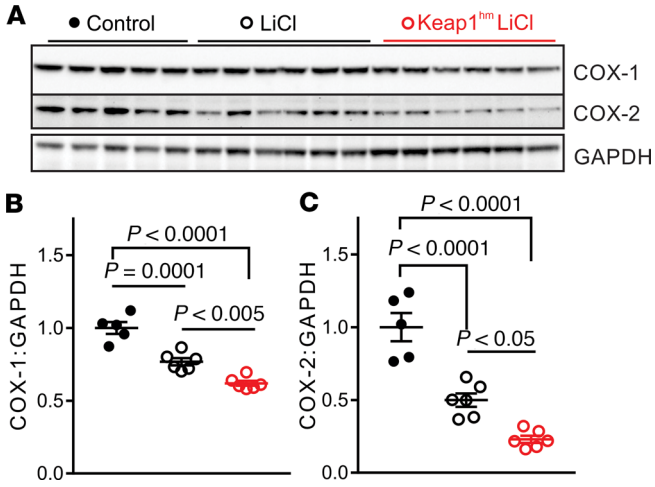

Figure 6. Constitutive Nrf2 activation suppresses COX-1 and COX-2. (**A**) Immunoblotting for COX-1 and COX-2 from kidneys of WT-Chow, WT-Li, and Keap1-Li mice. (**B** and **C**) Quantitative analysis of COX-1 and COX-2 expression by densitometry. Results showing individual values; *n* = 5–6, mean ± SEM with statistical analysis by 1-way ANOVA with Tukey correction for multiple comparisons.

expression in Keap1^{hm} mice correlated with a reduction in the renal levels of a stable prostacyclin (PGI_2) metabolite, 6-keto-$PGF_{1\alpha}$ (Supplemental Figure 10G). Together, these results suggest that constitutive graded Nrf2 activation reduces renal prostaglandin production.

Pharmacologic activation of Nrf2 with CDDO-Me protects against Li-NDI. The strong protective effect of genetic graded Nrf2 activation in Li-NDI motivated us to evaluate the viability of pharmacologic Nrf2 activation as a therapeutic intervention. CDDO-Me is a synthetic triterpenoid that potently activates Nrf2 and is in Phase II/III clinical trials for treatment of Alport Syndrome, a genetic disease characterized by progressive loss of kidney function (39), as well as other rare CKDs (38). Administration of CDDO-Me beginning 3 days prior to Li and continuing throughout Li exposure (Figure 7A) significantly reduced water intake and protected against weight loss without impacting food consumption (Figure 7, B–D) or reducing plasma Li^+ (Figure 7I) in WT mice. Similar to genetic Nrf2 hyperactivation via Keap1 hypomorphism, CDDO-Me increased renal NQO1 expression 2- to 3-fold (Figure 7, E and F). AQP2 abundance and glycosylation were not improved by CDDO-Me (Figure 7, E, G, and H), and urine osmolality showed only marginal improvement (Figure 7J), suggesting that pharmacologic and genetic activation both protect against Li-NDI via mechanisms unrelated to AQP2 expression.

To determine if genetic and pharmacologic mechanisms of protection converged, the expression of putative targets identified in Keap1^{hm} animals was evaluated in the CDDO-Me–treated cohort. Compared with vehicle-treated mice on Li diet, CDDO-Me modestly reduced tNCC abundance without impacting phosphorylation. NKCC2 and CA-II expression were unchanged by CDDO-Me. Li continued to induce downregulation of COX-1 and COX-2; however, pharmacologic Nrf2 activation did not have significant additional impact on expression of these proteins (Supplemental Figure 11).

Discussion

Li has remained a mainstay drug for mood stabilization in bipolar disorder for over half a century and is increasingly repurposed for treatment of other CNS diseases as new therapeutic effects are described and mechanisms documented (67). The beneficial effects of Li are complicated by adverse functional and structural renal sequelae. In addition to causing polyuria (>3,000 mL urine/day), chronic Li therapy can promote the development of CKD (7–11). Furthermore, Li has a narrow therapeutic index and is renally excreted, with CKD and other kidney injuries complicating the maintenance of plasma Li levels within a therapeutic range. As no alternatives match Li in efficacy of acute and chronic management of bipolar disorder and reduction of suicide risk (1), discontinuation poses a significant clinical challenge for nephrologists and psychiatrists caring for patients with this disease (68). Three-quarters of patients who are stable on Li have recurrent mood episodes within 5 years after discontinuation (69) and frequently require psychiatric hospitalization.

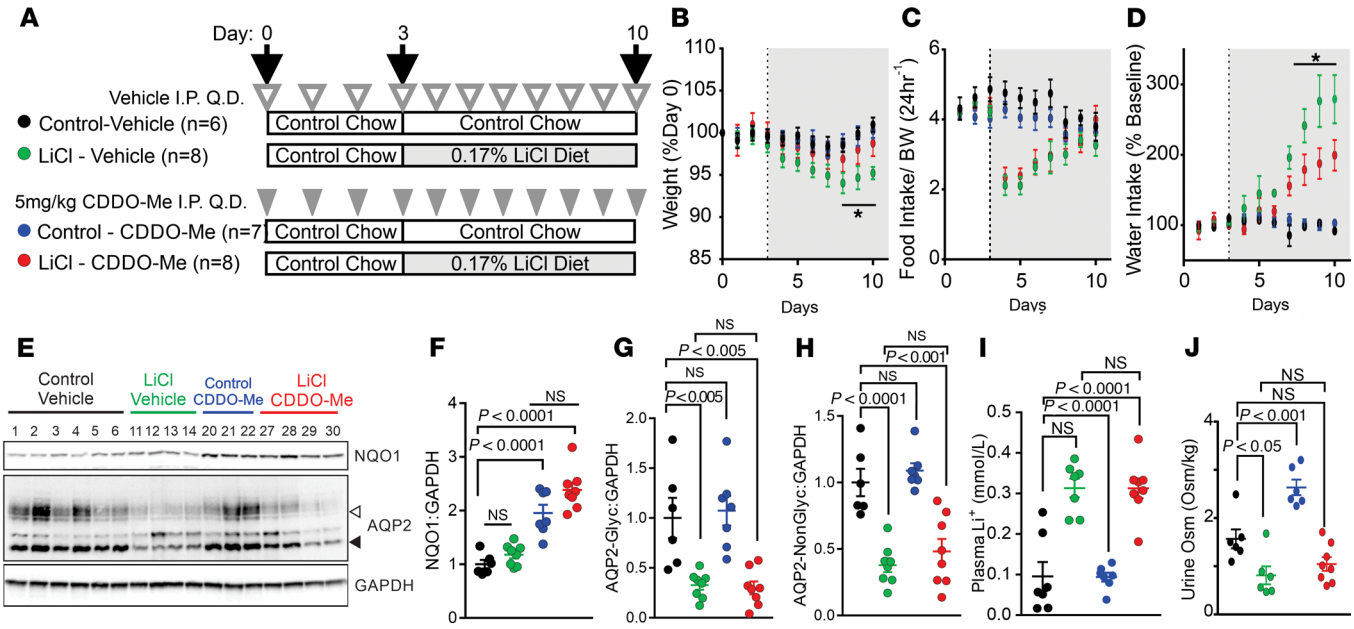

Figure 7. Pharmacologic activation of Nrf2 using CDDO-Me protects against polydipsia in Li-NDI via an AQP2-independent mechanism. (**A**) Schematic of the animal model of Li-NDI and treatment groups. All mice received normal chow for 0–3 days and were randomized to vehicle or CDDO-Me (5 mg/kg i.p., once per day [q.d.]). At day 3, mice were randomized to either normal chow or 0.17% LiCl diet. (**B**) Animal weights as a function of time, normalized to starting weight. (**C**) Twenty-four–hour food intake normalized to body weight. (**D**) Changes in water intake as a percentage of baseline expressed as mean ± SEM (n = 6–8 per group). *P < 0.05 denotes statistical significance compared with LiCl-vehicle by 2-way ANOVA with Dunnett correction for multiple comparisons. (**E**) Immunoblotting of whole-kidney lysates for glycosylated (white arrowhead, 30–42 kDa) and nonglycosylated (black arrowhead, 24 kDa) AQP2 and NQO1. (**F**–**H**) Densitometry showing individual values; mean ± SEM with statistical analysis by 1-way ANOVA with Tukey correction for multiple comparisons. (**I**) Plasma Li concentration. (**J**) Spot urine osmolality at day 10. Each point represents 1 animal in the study. Statistical significance by 2-way ANOVA with Dunnett correction for multiple comparisons.

Recent evidence implicates the Keap1/Nrf2 signaling pathway as playing a role in regulating AQP2 via as-of-yet known mechanisms. Specifically, hyperactivation of Nrf2 signaling by total ablation of its repressors Cul3, GSK3β, and Keap1 have independently been found to cause NDI in mice (18, 19, 26, 27). Surprisingly, we found that mice with Keap1 hypomorphism are protected against the development of Li-NDI, with complete normalization of water intake compared with WT mice receiving Li. In striking contrast to Keap1$^{-/-}$ animals (18, 19), Keap1^{hm} mice exhibited only mild hyposthenuria and polyuria at baseline and had normal urine concentrating ability and upregulation of plasma renin activity in response to 12-hour water deprivation. Thus, it is possible that Nrf2 activation displays hormesis (28), with activity above a certain threshold causing adverse outcomes (18, 19, 70).

The kidney has high energy requirements due to significant active transport mechanisms and, despite their small size (~0.5% body weight), consumes about ~10% of total oxygen used in cellular respiration. A gradient of glucose availability establishes from the renal cortex inward, resulting in low O_2 tension in the inner medulla and a predominantly anaerobic metabolism (71). In the context of the kidneys' high energetic demands and extensive xenobiotic exposure, the protective role of Nrf2 gains significance. It is intriguing that the spatial distribution of NQO1 expression in murine kidney appears to parallel the postulated O_2 and glucose gradients, with high cortical and low medullary abundance. Furthermore, NQO1 expression at baseline was significantly lower in DT epithelial cells than PT epithelial cells, and DT cells were more sensitive to both genetic activation and the electrophilic Nrf2 inducer CDDO-Me.

The renal damage caused by prolonged Li therapy is reversible in its early stages but may progress to irreversible deleterious remodeling and loss of function (9–11). Risk of progression to end-stage renal disease is significantly greater in patients on Li than in the general population, indicating a substantial unmet clinical need (5, 7). Existing therapeutic approaches for treating Li-NDI fall under 2 main categories: (a) diuretics or (b) inhibition of renal COX-1 and/or COX-2 with NSAIDs.

The diuretics acetazolamide (50–52), amiloride (12–14, 46–49), furosemide (61), and hydrochlorothiazide (41–45) have been found to paradoxically reduce urine output in Li-NDI. While all of these interventions have been documented to reduce polyuria/polydipsia, the underlying mechanisms remain unclear.

For instance, while in some studies acetazolamide increased cortical CD abundance of AQP2 (51), the reduction of polyuria appears independent of AQP2 expression levels (50). Similarly, thiazides were long thought to paradoxically reduce polyuria through their inhibition of NCC; however, recent evidence shows that this class of drugs also mitigates Li-NDI in NCC-KO animals (45). With the exception of amiloride, which directly reduces Li uptake, AQP2 protein abundance and urine osmolality are not consistently increased by any of these treatments, suggesting that they do not rescue cortical CD function. Based on this evidence, the protection is thought to involve modulation of TGF in conjunction with PT water reabsorption. Reduction of distal sodium reabsorption is believed to deplete extracellular volume, diminishing GFR and increasing proximal sodium and water reabsorption through effects on medullary osmolality and PT function (72). A major complication with existing diuretic therapies is that volume depletion complicates the dosing of Li (73, 74) and may interact with dosing of other pharmaceuticals. As such, diuretic use becomes complex in the setting of polypharmacy, and long-term diuretic prophylaxis is not used clinically to prevent Li-NDI.

COX inhibitors (e.g., NSAIDs) have been used as a last-resort therapeutic for Li-NDI patients (53–55, 75), despite the documented risk of renal hypoperfusion and AKI associated with this class of drugs (76, 77). Notably, mice lacking the microsomal prostaglandin E synthase-1 (mPGES-1) were also found to be resistant to Li-NDI (78). In our study, downregulation of NCC, NKCC2, and CA-II expression in Keap1^{hm} mice suggests potential overlapping mechanisms of action between Nrf2 activation and the diuretics, which target these proteins. Furthermore, we demonstrated that renal COX-1 and COX-2 expression are reduced in Keap1^{hm} mice at both the mRNA and protein levels. While expression of COX-1 and COX-2 are not known to be directly dependent on upstream antioxidant response element (ARE), COX-2 has been shown to be upregulated in Nrf2$^{-/-}$ mice (79). In our study, the reduction in COX expression correlates with diminished production of the vasodilator PGI_2. Together, these results indicate that activation of Nrf2 may modulate TGF via alteration of distal sodium reabsorption and vasodilator biosynthesis. Importantly, Nrf2 activation did not affect plasma Li^+ concentration. This property differentiates Nrf2 from diuretics and suggests that Nrf2 therapy may be suitable for long-term coadministration with Li and NDI prophylaxis.

Our study demonstrates that Nrf2 activators may offer a therapeutic approach for Li-NDI treatment. Preclinical studies have shown that pharmacologic or genetic activation of Nrf2 can protect against acute and chronic kidney diseases by protecting cells from oxidative injury and reducing fibrotic remodeling. Rodent models of CKD have implicated Nrf2 deficiency as an important component of disease etiology (80–82). Mice with constitutive hyperactivation of Nrf2 activity induced by genetic hypomorphism of Keap1 are protected against CKD and fibrosis after obstructive and ischemic AKI (31, 83). Encouragingly, pharmacologic activators of Nrf2 have cleared Phase I safety studies and are undergoing Phase II/III clinical trials for treatment of CKD (CXA-10 and CDDO-Me, respectively). Coadministration of Nrf2 activators with Li may present a unique window of opportunity for primary prevention of renal injury in the setting of chronic Li use and could prolong the clinical efficacy and safety of Li therapy for patients with bipolar disorder.

Summary statement. Our results demonstrate that activation of the Keap1/Nrf2 signaling pathway completely protects mice from polydipsia/polyuria in Li-NDI. The reduction in polydipsia occurs without altering AQP2 expression or increasing urine osmolality. Activation of Nrf2 decreased the expression of NCC, NKCC2, and CA-II, mimicking the effects of diuretic therapies for Li-NDI. Vascular effects of Nrf2 activation may serve as additional contributory mechanisms through decreased expression and activity of COX. Pharmacologic activation of Nrf2 with CDDO-Me validated this pathway as a potential therapeutic target for Li-NDI. Our findings show that Nrf2 agonists have the potential to protect against development of NDI and may ultimately protect against the long-term sequela of fibrotic remodeling and CKD associated with chronic Li therapy.

Methods

Materials. Acetylcholine and sodium nitroprusside (SNP) were purchased from MilliporeSigma. Solvents were liquid chromatography–mass spectrometry (LC-MS) grade from Burdick and Jackson. Chemicals were of analytical grade and purchased from MilliporeSigma unless otherwise stated. CDDO-Me and CDDO-Im were from Toronto Research Chemicals. Primary antibodies were purchased from the following suppliers: NQO1 (ab34173, Abcam), GAPDH (2275PC100, Trevigen), COX-1 (4841S, Cell Signaling Technology), COX-2 (ab15191 or ab179800, Abcam), MUC1 (MA5-11202, Thermo Fisher Scientific), CD10 (MA5-14050, Thermo Fisher Scientific), ENaC α/β/γ (SPC-403, SPC-404, SPC-405, respectively; StressMarq), NCC (ab95302, Abcam), phospho-NCC (T53, PhosphoSolutions), Carbonic Anhydrase II (Abcam), AQP1 (ab15080, Abcam), AQP2 (H7661; gift of Robert Fenton, Aarhus University, Denmark).

Secondary antibodies were purchased from Santa Cruz Biotechnologies. Angiotensinogen 1–14, (rat sequence, DRVYIHPFHLLYYS) and $^{13}C/^{15}N$-labeled Angiotensin I (DR-V*-Y-I*-HPFHL) were obtained from AnaSpec. MiniTab protease and Phos-Stop phosphatase inhibitor cocktails were from Roche. Isotopically labeled standard 6-keto PGF1α-d4 was from Cayman Chemical.

Animals. Male C57BL/6J albino mice (the Jackson Laboratory, JAX000058) at 8 weeks of age were habituated to individual housing for 4 days, followed by randomization to receive control diet or a diet containing 0.17% LiCl by weight (Teklad) ad libitum. Water was provided ad libitum. Mice were maintained on a 12-hour light/12-hour dark cycle. After 7 days, mice were sacrificed by terminal exsanguination under isoflurane anesthesia. A blood sample was collected by retroorbital bleeding, after which a laparotomy and thoracotomy were performed. A hemostat was applied to the left renal vascular bundle, and the left kidney was removed and flash-frozen in liquid nitrogen. The vena cava was severed, and whole-animal transcardial perfusion was performed with cold 2% PFA in PBS. The right kidney was removed, bisected, and fixed in 2% PFA for 1.5 hours, followed by dehydration in 30% sucrose for 24 hours and freezing in OCT compound. Twelve-hour water deprivation was performed overnight, 8 pm to 8 am, after which time animals were euthanized and tissues collected as above. Metabolic cage urine collection was performed for 24 hours with food and water ad libitum. For sodium depletion or sodium loading, diet containing 0.01%–0.02% Na or 1.6% Na (Teklad) were provided for a period of 2 weeks prior to sacrifice.

Water and urine. Mice and food were weighed daily. Water was supplied in 50 mL conical with sipper tube as described (http://www.bio-protocol.org/e1822), and daily water intake was determined by weight. Spot urine was collected after spontaneous voiding on plastic wrap, and urine osmolality was measured in technical duplicate with Wescor 5500 Vapor Pressure Osmometer using 10 μL urine; the average value was reported each mouse.

Cell culture. Whole adult human kidneys were obtained via the Center for Organ Recovery and Education (CORE; Pittsburgh, Pennsylvania, USA) from donation-after-cardiac-death or brain-dead donors that were not accepted for transplant. Primary human proximal and DT cells were immunoaffinity isolated from human adult kidneys using antibodies against CD13 (proximal) and Muc1 (distal) and cultured as previously described (59). Confluent monolayers of cells were incubated with vehicle control, LiCl, or CDDO-Im for 18 hours in serum-free hormonally defined media, followed by preparation of lysates for immunoblotting.

qPCR. Total RNA was extracted using TRIzol (Invitrogen) and subjected to reverse transcription with the iScript cDNA synthesis kit. The TaqMan gene expression assays-on-demand system (Applied Biosystems) was used for gene expression assessment by quantitative PCR (qPCR) using GAPDH as housekeeping gene.

Immunoblotting. Flash-frozen kidneys were homogenized in ice-cold RIPA buffer containing protease and phosphatase inhibitor cocktails. Cells were treated as indicated. At the time of collection, cells were washed 2 times with cold PBS and lysates were prepared in 4°C lysis buffer containing protease inhibitors. Protein was quantified by BCA assay (Pierce), and a sample containing 15–25 μg total cellular protein was loaded on 4%–12% reducing Bis-Tris gel (NuPage, Invitrogen). Resolved proteins were transferred to 0.45 μm nitrocellulose membrane (Bio-Rad) and blocked with 5% nonfat dry milk (LabScientific) or 5% BSA (MilliporeSigma) in TBS-0.1% Tween 20 (Thermo Fisher Scientific) for 1 hour. Membranes were incubated with primary antibody (1:1000 dilution) for 1 hour at room temperature (RT) or overnight at 4°C. The appropriate secondary antibody was applied at dilution of 1:5000 for 1 hour, the membrane was washed three times in TBS-0.1% Tween-20, and the membrane was visualized with Clarity ECL chemiluminescence kit and ChemiDoc imager (Bio-Rad). Quantitative densitometric analysis was performed using NIH ImageJ, with individual band intensities normalized to housekeeping protein abundance and mean of control group normalized to 1.

Immunofluorescence. Kidney cryostat sections (5 μm) were washed 3 times with PBS, followed by 3 washes with solution of 0.5% BSA in PBS. Sections were blocked with 5% normal goat serum in BSA solution for 45 minutes. The slides were incubated for 1 hour at RT with primary antibodies for rabbit anti-NQ01 (ab34173, Abcam) at 1:500 and hamster anti-MUC1 (MA5-11202, Thermo Fisher Scientific) at 1:50 in 0.5% BSA solution. Slides were washed 3 times with BSA solution and incubated for 1 hour at RT with Alexa 488 donkey anti-mouse secondary antibody (A21202, Invitrogen) diluted 1:500, combined with goat anti–rabbit CY5 (111-605-003, Jackson ImmunoResearch) 1:1000, and goat anti–hamster Cy3 (127-165-160, Jackson ImmunoResearch) combined with 1:500 Alexa 488 phalloidin (A12379, Thermo Fisher Scientific) in BSA solution. Nuclei were stained with Hoechst dye (bisbenzamide 1 mg/100 mL water) for 30 seconds. After 3 rinses with PBS, sections were coverslipped with gelvatol mounting media. Images were captured with a Nikon A1 confocal microscope (NIS Elements 4.4)

Plasma renin activity assay. A total of 30 μL plasma was added to 270 μL generation buffer (1.0 M Tris, 0.25 M EDTA, 1 mM phenylmethylsulfonyl fluoride [PMSF, MilliporeSigma], pH 5.5) containing 30 μM Angiotensinogen 1–14 renin substrate (and the reaction was incubated at 37°C). A total of 50 μL aliquots were removed at 0, 10, 20, and 30 minutes and quenched with 200 μL MeOH containing 3% formic acid and $^{13}C/^{15}N$-labeled Angiotensin I (AngI) internal standard. The solution was chilled at –20°C, and protein precipitates were removed by centrifugation 16,000 *g* for 10 minutes. A total of 20 μL of supernatant was injected for High-performance LC–tandem MS (HPLC-MS/MS) analysis.

HPLC-MS/MS. A Shimadzu HPLC coupled to a Thermo Fisher Scientific CTC HTS PAL autosampler and an AB Sciex 5000 triple quadrupole mass spectrometer was used for the quantification of AngI, isotopic AngI standard, and angiotensinogen (Agt). Peptides were resolved on a Phenomenex Gemini C18 column (2.0 × 20 mm, 3 μm pore size) using a binary solvent system consisting of aqueous 0.1% formic acid (solvent A) and 0.1% formic acid in acetonitrile (solvent B) at a flow rate of 850 μL/min. Chromatographic conditions were as follows: 5% solvent B for 0.3 minutes, followed by a linear gradient to 45% solvent B at 2.5 minutes; this then moved to 100% solvent B for 1 minute, followed by reequilibration, to return to the initial condition (5% solvent B) for 4.5 minutes. The triple quadrupole mass spectrometer was tuned and used in positive ion mode with the following settings: source temperature 650°C; ionization spray voltage 5000 V; CAD 5.0 AU; curtain gas 40 AU; GS1 55 AU; GS2 55 AU; EP 10.00V; CXP 10.00 V. Multiple reaction monitoring was performed with 75 ms dwell time and declustering potential 100 V; collision energy 30–37 V was performed using the following transitions: Ang I (Q1 433.20 → Q3 110.20), isotopic Ang I (Q1 655.60 → Q3 110.20), Agt (Q1 608.50 → Q3 269.20). Sample AngI was calculated based on area ratio and calibration curves prepared using commercially available AngI standards, and plasma renin activity (PRC) was determined from slope of AngI generated by each sample as a function of time.

Determination of 6-keto prostaglandin F1α. Flash-frozen kidney samples were weighed on an analytical balance and transferred to chilled Eppendorf tubes containing equivalent weight of zirconium oxide homogenization beads. A total of 380 μL distilled water containing isotopically labeled standard 6-keto PGF1α-d4 (Cayman Chemical) (final concentration 50 ng/mL) was added to each sample and homogenized at 4°C using a Bullet Blender (Next Advance). The lysate was added to 1.6 mL acetonitrile and centrifuged at 21,100 *g* for 15 minutes at 4°C. The supernatant was transferred to a clean glass tube and dried under N_2 (gas) for 1 hour. Samples were resuspended in 200 μL MeOH, and 10 μL was injected for HPLC-MS/MS analysis. Then, 6-keto PGF1α was quantified using a 6-point calibration curve prepared for each experiment. The 6-keto-PGF1α was chromatographically resolved on a Phenomenex Kinetex C18 column (2.1 × 150 mm, 5 μm pore size) using aqueous 0.1% ammonium acetate (solvent A) and 0.1% ammonium acetate in acetonitrile (solvent B) at a total flow of 0.25 mL/min. Solvent B was increased from 10% to 65% solvent B over 20 minutes, followed by a 3-minute wash with 100% solvent B and return to 10% solvent B for 2 minutes, for a total run time of 25 minutes. The following settings were used in negative ion mode: source temperature 650°C; ionization spray voltage 5000 V; CAD 5.0 AU; curtain gas 40 AU; GS1 55 AU; GS2 55 AU; EP –5.00 V; CXP –18.40 V. Multiple reaction monitoring was performed with 150 ms dwell time and declustering potential –50 V; collision energy –17 V was performed using the following transitions: 6-keto PGF1α (Q1 369.10 → Q3 245.00), 6-keto PGF1α-*d4* (Q1 373.1 → Q3 167.00).

Statistics. Statistical analysis was performed in GraphPad Prism 7. Data were analyzed using 2-tailed Student's *t* test and repeated-measures 1-way or 2-way ANOVA with Tukey-Kramer or Dunnett post hoc tests, as indicated in figure legends. $P < 0.05$ was considered statistically significant; *P* values are disclosed in figures and figure legends.

Study approval. All animal experiments were performed with the approval of the University of Pittsburgh's IACUC. Primary human renal cortical cells were obtained from CORE under approval by the University of Pittsburgh Committee for Oversight of Research and Clinical Training Involving Decedents (CORID), project 462.

Author contributions

SJ, DAV, and FJS conceived and designed the study. SJ, DAV, SRS, MFP, PR, DRE, and MR performed experiments and performed analyses. SH, CSC, SGW, and ACS contributed technical expertise, data analysis, and tools. SJ, DAV, and FJS wrote the manuscript. ARS and RJT contributed critical revisions of the manuscript. FJS supervised all aspects of the project. All authors agreed to the content of the submitted manuscript.

Acknowledgments

We would like to thank Thomas Kensler for providing breeding pairs of Keap1^{hm} and Nrf2$^{-/-}$ mice. We acknowledge the CORE for the provision of human kidneys for research. We would like to thank Bruce Freeman for insightful advice. This work was supported by NIH 5F30DK108391 (to SJ); R01-GM125944 and R01-DK112854 (to FJS); AHA 17GRN33660955 (to FJS); K01-HL133331; the Vascular Medicine Institute; the Hemophilia Center of Western Pennsylvania (to DAV, ACS); the Institute for Transfusion Medicine (to DAV, ACS); R21AI122071 (to SGW); AHA FTF 16990086 and ASN Carl W. Gottschalk Research Scholar Grant (to RJT); NIH P30-DK079307 (to the Pittsburgh Center for Kidney Research); R01-DK098145 (to ARS); R01-HL133864 and R01-HL128304 (to ACS); and AHA American Heart Association Established Investigator Grant 19 EIA34770095 (to ACS).

Address correspondence to: Francisco Jose Schopfer, E1316 BST. 200 Lothrop, St. Pittsburgh, Pennsulvania 15213, USA. Phone: 412.648.0193; email: fjs2@pitt.edu.

1. Song J, et al. Suicidal Behavior During Lithium and Valproate Treatment: A Within-Individual 8-Year Prospective Study of 50,000 Patients With Bipolar Disorder. *Am J Psychiatry*. 2017;174(8):795–802.
2. Gitlin M. Lithium side effects and toxicity: prevalence and management strategies. *Int J Bipolar Disord*. 2016;4(1):27.
3. Boton R, Gaviria M, Batlle DC. Prevalence, pathogenesis, and treatment of renal dysfunction associated with chronic lithium therapy. *Am J Kidney Dis*. 1987;10(5):329–345.
4. Grünfeld JP, Rossier BC. Lithium nephrotoxicity revisited. *Nat Rev Nephrol*. 2009;5(5):270–276.
5. Close H, et al. Renal failure in lithium-treated bipolar disorder: a retrospective cohort study. *PLoS ONE*. 2014;9(3):e90169.
6. Kessing LV, Gerds TA, Feldt-Rasmussen B, Andersen PK, Licht RW. Use of Lithium and Anticonvulsants and the Rate of Chronic Kidney Disease: A Nationwide Population-Based Study. *JAMA Psychiatry*. 2015;72(12):1182–1191.
7. Aiff H, Attman PO, Aurell M, Bendz H, Schön S, Svedlund J. End-stage renal disease associated with prophylactic lithium treatment. *Eur Neuropsychopharmacol*. 2014;24(4):540–544.
8. Aiff H, et al. Effects of 10 to 30 years of lithium treatment on kidney function. *J Psychopharmacol (Oxford)*. 2015;29(5):608–614.
9. Rabin EZ, Garston RG, Weir RV, Posen GA. Persistent nephrogenic diabetes insipidus associated with long-term lithium carbonate treatment. *Can Med Assoc J*. 1979;121(2):194–198.
10. Cairns SR, Wolman R, Lewis JG, Thakker R. Persistent nephrogenic diabetes insipidus, hyperparathyroidism, and hypothyroidism after lithium treatment. *Br Med J (Clin Res Ed)*. 1985;290(6467):516–517.
11. Garofeanu CG, Weir M, Rosas-Arellano MP, Henson G, Garg AX, Clark WF. Causes of reversible nephrogenic diabetes insipidus: a systematic review. *Am J Kidney Dis*. 2005;45(4):626–637.
12. Kosten TR, Forrest JN. Treatment of severe lithium-induced polyuria with amiloride. *Am J Psychiatry*. 1986;143(12):1563–1568.
13. Kortenoeven ML, et al. Amiloride blocks lithium entry through the sodium channel thereby attenuating the resultant nephrogenic diabetes insipidus. *Kidney Int*. 2009;76(1):44–53.
14. Christensen BM, et al. alphaENaC-mediated lithium absorption promotes nephrogenic diabetes insipidus. *J Am Soc Nephrol*. 2011;22(2):253–261.
15. Marples D, Christensen S, Christensen EI, Ottosen PD, Nielsen S. Lithium-induced downregulation of aquaporin-2 water channel expression in rat kidney medulla. *J Clin Invest*. 1995;95(4):1838–1845.
16. Kwon TH, et al. Altered expression of renal AQPs and Na(+) transporters in rats with lithium-induced NDI. *Am J Physiol Renal Physiol*. 2000;279(3):F552–F564.
17. Thomsen K, Shirley DG. A hypothesis linking sodium and lithium reabsorption in the distal nephron. *Nephrol Dial Transplant*. 2006;21(4):869–880.
18. Noel S, Arend LJ, Bandapalle S, Reddy SP, Rabb H. Kidney epithelium specific deletion of kelch-like ECH-associated protein 1 (Keap1) causes hydronephrosis in mice. *BMC Nephrol*. 2016;17(1):110.
19. Suzuki T, et al. Hyperactivation of Nrf2 in early tubular development induces nephrogenic diabetes insipidus. *Nat Commun*. 2017;8:14577.
20. Itoh K, et al. An Nrf2/small Maf heterodimer mediates the induction of phase II detoxifying enzyme genes through antioxidant response elements. *Biochem Biophys Res Commun*. 1997;236(2):313–322.
21. Alam J, Stewart D, Touchard C, Boinapally S, Choi AM, Cook JL. Nrf2, a Cap'n'Collar transcription factor, regulates induction of the heme oxygenase-1 gene. *J Biol Chem*. 1999;274(37):26071–26078.
22. Ishii T, et al. Transcription factor Nrf2 coordinately regulates a group of oxidative stress-inducible genes in macrophages. *J Biol Chem*. 2000;275(21):16023–16029.
23. Itoh K, Tong KI, Yamamoto M. Molecular mechanism activating Nrf2-Keap1 pathway in regulation of adaptive response to electrophiles. *Free Radic Biol Med*. 2004;36(10):1208–1213.
24. Kobayashi M, et al. The antioxidant defense system Keap1-Nrf2 comprises a multiple sensing mechanism for responding to a wide range of chemical compounds. *Mol Cell Biol*. 2009;29(2):493–502.
25. Takaya K, et al. Validation of the multiple sensor mechanism of the Keap1-Nrf2 system. *Free Radic Biol Med*. 2012;53(4):817–827.
26. McCormick JA, et al. Hyperkalemic hypertension-associated cullin 3 promotes WNK signaling by degrading KLHL3. *J Clin Invest*. 2014;124(11):4723–4736.
27. Rao R, Patel S, Hao C, Woodgett J, Harris R. GSK3beta mediates renal response to vasopressin by modulating adenylate cyclase activity. *J Am Soc Nephrol*. 2010;21(3):428–437.
28. Castillo-Quan JI, et al. Lithium Promotes Longevity through GSK3/NRF2-Dependent Hormesis. *Cell Rep*. 2016;15(3):638–650.

29. Alural B, Ozerdem A, Allmer J, Genc K, Genc S. Lithium protects against paraquat neurotoxicity by NRF2 activation and miR-34a inhibition in SH-SY5Y cells. *Front Cell Neurosci*. 2015;9:209.
30. Chen X, et al. GSK-3β downregulates Nrf2 in cultured cortical neurons and in a rat model of cerebral ischemia-reperfusion. *Sci Rep*. 2016;6:20196.
31. Tan RJ, et al. Keap1 hypomorphism protects against ischemic and obstructive kidney disease. *Sci Rep*. 2016;6:36185.
32. Ruiz S, Pergola PE, Zager RA, Vaziri ND. Targeting the transcription factor Nrf2 to ameliorate oxidative stress and inflammation in chronic kidney disease. *Kidney Int*. 2013;83(6):1029–1041.
33. Martini S, et al. Integrative biology identifies shared transcriptional networks in CKD. *J Am Soc Nephrol*. 2014;25(11):2559–2572.
34. Liu M, et al. The Nrf2 triterpenoid activator, CDDO-imidazolide, protects kidneys from ischemia-reperfusion injury in mice. *Kidney Int*. 2014;85(1):134–141.
35. Miyazaki Y, et al. Keap1 inhibition attenuates glomerulosclerosis. *Nephrol Dial Transplant*. 2014;29(4):783–791.
36. Choi BH, Kang KS, Kwak MK. Effect of redox modulating NRF2 activators on chronic kidney disease. *Molecules*. 2014;19(8):12727–12759.
37. Chin MP, et al. Bardoxolone Methyl Improves Kidney Function in Patients with Chronic Kidney Disease Stage 4 and Type 2 Diabetes: Post-Hoc Analyses from Bardoxolone Methyl Evaluation in Patients with Chronic Kidney Disease and Type 2 Diabetes Study. *Am J Nephrol*. 2018;47(1):40–47.
38. A Phase 2 Trial of the Safety and Efficacy of Bardoxolone Methyl in Patients With Rare Chronic Kidney Diseases - PHOENIX (PHOENIX). http://clinicaltrials.gov. NCT03366337. Accessed December 2, 2019.
39. Reata Pharmaceuticals. A Phase 2/3 Trial of the Efficacy and Safety of Bardoxolone Methyl in Patients With Alport Syndrome - CARDINAL (CARDINAL). http://clinicaltrials.gov. NCT03019185. Accessed December 2, 2019.
40. Complexa. FIRSTx - A Study of Oral CXA-10 in Primary Focal Segmental Glomerulosclerosis (FSGS). http://clinicaltrials.gov. NCT03422510. Accessed December 2, 2019.
41. Shirley DG, Walter SJ, Laycock JF. The antidiuretic effect of chronic hydrochlorothiazide treatment in rats with diabetes insipidus: renal mechanisms. *Clin Sci*. 1982;63(6):533–538.
42. Walter SJ, Skinner J, Laycock JF, Shirley DG. The antidiuretic effect of chronic hydrochlorothiazide treatment in rats with diabetes insipidus: water and electrolyte balance. *Clin Sci*. 1982;63(6):525–532.
43. Konoshita T, et al. Treatment of congenital nephrogenic diabetes insipidus with hydrochlorothiazide and amiloride in an adult patient. *Horm Res*. 2004;61(2):63–67.
44. Kim GH, et al. Antidiuretic effect of hydrochlorothiazide in lithium-induced nephrogenic diabetes insipidus is associated with upregulation of aquaporin-2, Na-Cl co-transporter, and epithelial sodium channel. *J Am Soc Nephrol*. 2004;15(11):2836–2843.
45. Sinke AP, et al. Hydrochlorothiazide attenuates lithium-induced nephrogenic diabetes insipidus independently of the sodium-chloride cotransporter. *Am J Physiol Renal Physiol*. 2014;306(5):F525–F533.
46. Finch CK, Kelley KW, Williams RB. Treatment of lithium-induced diabetes insipidus with amiloride. *Pharmacotherapy*. 2003;23(4):546–550.
47. Bedford JJ, et al. Amiloride restores renal medullary osmolytes in lithium-induced nephrogenic diabetes insipidus. *Am J Physiol Renal Physiol*. 2008;294(4):F812–F820.
48. Bedford JJ, et al. Lithium-induced nephrogenic diabetes insipidus: renal effects of amiloride. *Clin J Am Soc Nephrol*. 2008;3(5):1324–1331.
49. Kalita-De Croft P, Bedford JJ, Leader JP, Walker RJ. Amiloride modifies the progression of lithium-induced renal interstitial fibrosis. *Nephrology (Carlton)*. 2018;23(1):20–30.
50. de Groot T, et al. Lithium-induced NDI: acetazolamide reduces polyuria but does not improve urine concentrating ability. *Am J Physiol Renal Physiol*. 2017;313(3):F669–F676.
51. de Groot T, et al. Acetazolamide Attenuates Lithium-Induced Nephrogenic Diabetes Insipidus. *J Am Soc Nephrol*. 2016;27(7):2082–2091.
52. Gordon CE, Vantzelfde S, Francis JM. Acetazolamide in Lithium-Induced Nephrogenic Diabetes Insipidus. *N Engl J Med*. 2016;375(20):2008–2009.
53. Allen HM, Jackson RL, Winchester MD, Deck LV, Allon M. Indomethacin in the treatment of lithium-induced nephrogenic diabetes insipidus. *Arch Intern Med*. 1989;149(5):1123–1126.
54. Lam SS, Kjellstrand C. Emergency treatment of lithium-induced diabetes insipidus with nonsteroidal anti-inflammatory drugs. *Ren Fail*. 1997;19(1):183–188.
55. Kim GH, et al. Treating lithium-induced nephrogenic diabetes insipidus with a COX-2 inhibitor improves polyuria via upregulation of AQP2 and NKCC2. *Am J Physiol Renal Physiol*. 2008;294(4):F702–F709.
56. Kim GH. Renal effects of prostaglandins and cyclooxygenase-2 inhibitors. *Electrolyte Blood Press*. 2008;6(1):35–41.
57. Taguchi K, Maher JM, Suzuki T, Kawatani Y, Motohashi H, Yamamoto M. Genetic analysis of cytoprotective functions supported by graded expression of Keap1. *Mol Cell Biol*. 2010;30(12):3016–3026.
58. Kalliokoski O, et al. Mice do not habituate to metabolism cage housing--a three week study of male BALB/c mice. *PLoS ONE*. 2013;8(3):e58460.
59. Emlet DR, et al. Insulin-like growth factor binding protein 7 and tissue inhibitor of metalloproteinases-2: differential expression and secretion in human kidney tubule cells. *Am J Physiol Renal Physiol*. 2017;312(2):F284–F296.
60. Ma T, Yang B, Gillespie A, Carlson EJ, Epstein CJ, Verkman AS. Severely impaired urinary concentrating ability in transgenic mice lacking aquaporin-1 water channels. *J Biol Chem*. 1998;273(8):4296–4299.
61. Michimata M, et al. Reverse pharmacological effect of loop diuretics and altered rBSC1 expression in rats with lithium nephropathy. *Kidney Int*. 2003;63(1):165–171.
62. Kim YH, et al. Altered expression of renal acid-base transporters in rats with lithium-induced NDI. *Am J Physiol Renal Physiol*. 2003;285(6):F1244–F1257.
63. Mukherjee M, et al. Endogenous Notch Signaling in Adult Kidneys Maintains Segment-Specific Epithelial Cell Types of the Distal Tubules and Collecting Ducts to Ensure Water Homeostasis. *J Am Soc Nephrol*. 2019;30(1):110–126.
64. Aubert S, et al. MUC1, a new hypoxia inducible factor target gene, is an actor in clear renal cell carcinoma tumor progression.

Cancer Res. 2009;69(14):5707–5715.
65. Braga VM, Pemberton LF, Duhig T, Gendler SJ. Spatial and temporal expression of an epithelial mucin, Muc-1, during mouse development. *Development*. 1992;115(2):427–437.
66. Pastor-Soler NM, et al. Muc1 is protective during kidney ischemia-reperfusion injury. *Am J Physiol Renal Physiol*. 2015;308(12):F1452–F1462.
67. Young AH. More good news about the magic ion: lithium may prevent dementia. *Br J Psychiatry*. 2011;198(5):336–337.
68. Goodwin GM. The Safety of Lithium. *JAMA Psychiatry*. 2015;72(12):1167–1169.
69. Faedda GL, Tondo L, Baldessarini RJ, Suppes T, Tohen M. Outcome after rapid vs gradual discontinuation of lithium treatment in bipolar disorders. *Arch Gen Psychiatry*. 1993;50(6):448–455.
70. Yoshida E, et al. Hyperactivation of Nrf2 leads to hypoplasia of bone in vivo. *Genes Cells*. 2018;23(5):386–392.
71. Chen Y, Fry BC, Layton AT. Modeling Glucose Metabolism in the Kidney. *Bull Math Biol*. 2016;78(6):1318–1336.
72. Magaldi AJ. New insights into the paradoxical effect of thiazides in diabetes insipidus therapy. *Nephrol Dial Transplant*. 2000;15(12):1903–1905.
73. Finley PR, Warner MD, Peabody CA. Clinical relevance of drug interactions with lithium. *Clin Pharmacokinet*. 1995;29(3):172–191.
74. Finley PR. Drug Interactions with Lithium: An Update. *Clin Pharmacokinet*. 2016;55(8):925–941.
75. Tran-Van D, Avargues P, Labadie P, Hervé Y, Dardare E, Fontaine B. [Intravenous ketoprofen for severe lithium-induced polyuria]. *Presse Med*. 2005;34(16 Pt 1):1137–1140.
76. Brater DC, Harris C, Redfern JS, Gertz BJ. Renal effects of COX-2-selective inhibitors. *Am J Nephrol*. 2001;21(1):1–15.
77. Ungprasert P, Cheungpasitporn W, Crowson CS, Matteson EL. Individual non-steroidal anti-inflammatory drugs and risk of acute kidney injury: A systematic review and meta-analysis of observational studies. *Eur J Intern Med*. 2015;26(4):285–291.
78. Jia Z, Wang H, Yang T. Mice lacking mPGES-1 are resistant to lithium-induced polyuria. *Am J Physiol Renal Physiol*. 2009;297(6):F1689–F1696.
79. Khor TO, Huang MT, Kwon KH, Chan JY, Reddy BS, Kong AN. Nrf2-deficient mice have an increased susceptibility to dextran sulfate sodium-induced colitis. *Cancer Res*. 2006;66(24):11580–11584.
80. Kim HJ, Vaziri ND. Contribution of impaired Nrf2-Keap1 pathway to oxidative stress and inflammation in chronic renal failure. *Am J Physiol Renal Physiol*. 2010;298(3):F662–F671.
81. Kim HJ, Sato T, Rodríguez-Iturbe B, Vaziri ND. Role of intrarenal angiotensin system activation, oxidative stress, inflammation, and impaired nuclear factor-erythroid-2-related factor 2 activity in the progression of focal glomerulosclerosis. *J Pharmacol Exp Ther*. 2011;337(3):583–590.
82. Aminzadeh MA, Nicholas SB, Norris KC, Vaziri ND. Role of impaired Nrf2 activation in the pathogenesis of oxidative stress and inflammation in chronic tubulo-interstitial nephropathy. *Nephrol Dial Transplant*. 2013;28(8):2038–2045.
83. Nezu M, et al. Transcription factor Nrf2 hyperactivation in early-phase renal ischemia-reperfusion injury prevents tubular damage progression. *Kidney Int*. 2017;91(2):387–401.